Prediction of Porous Trailing Edge Noise Reduction via Acoustic Perturbation Equations and Volume Averaging

B. W. Faßmann* C. Rautmann† R. Ewert‡

J. W. Delfs§

German Aerospace Center (DLR), D-38108 Braunschweig, Germany

Edge noise is generated if turbulence interacts with solid edges. Reduction of trailing edge noise of airfoils can be achieved by replacing the solid material at the trailing edge by inlays of porous permeable material. The acoustic benefit of approximately 6 dB of such treatment is known from experiments. Enroute to numerically optimized porous properties, this paper presents a first principle based Computational Aeroacoustics (CAA) method for predicting the acoustic effect of a porous NACA0012 trailing edge. In a hybrid two-step CFD/CAA procedure the turbulence statistics from a solution of the Volume Averaged Navier-Stokes (VANS) equations is used as a basis for the prediction of turbulent-boundary-layer trailing-edge noise (TBL-TEN). For the acoustic part of the calculation, the Acoustic Perturbation Equations (APE) are solved in the flow field. Inside the porous regions, a different set of governing equations, referred to as Linear Perturbation Equations (LPE) will be solved. The LPE represent a modified form of the Linearized Euler Equations (LEE) with the APE vorticity source term shifted to the right-hand side. The new set of equations is derived by volume averaging the Navier-Stokes equations and decomposing the flow variables into a time-averaged mean part and a fluctuating part and isolating the vorticity source term to the right-hand side of the momentum equation. The LPE are verified by an analytical solution. The simulation results of a NACA0012 airfoil geometry with and without porous trailing edge treatment are compared to wind tunnel measurements. The noise reduction effect of such a trailing edge treatment is successfully demonstrated.

I. Introduction

In the field of aircraft application, future prospective short range aircraft with short take-off and landing (STOL) properties involve non-conventional high lift systems such as overblown flaps taking advantage of the coanda effect.[1] In this context, additional sound generation must be avoided. In 1979, Hayden investigated several edge concepts for overblown flaps.[2] Later, Howe[3] presented a basic theory on this. Besides trailing-edge shape modifications similar to serrations, Hayden and Chanaud[4] demonstrated that the application of porous material is reducing trailing edge noise. The positive effect of lengthwise slits applied to the trailing edge was shown in Ref. 5. The resulting reduction is about 6 dB compared to the solid reference. As the manufacturing of narrow slits is expensive, it is of strong interest to investigate the acoustic benefit of rigid, porous permeable material, e.g. sintered metal fiber felts or metal foams. Different porous materials were applied to the trailing edge of a high lift airfoil and aeroacoustically tested by Herr et al.[6] Maximal sound reduction of about 6 dB to 8 dB is reported. The authors have also demonstrated experimentally that a suppression of the ventilation of acoustic fluctuations (from one side of the airfoil to the other) by means of a tape attached to the pressure side of the porous trailing edge of a cambered airfoil entirely degrades the acoustic benefit.

*Research Scientist, AIAA Member, Corresponding Author benjamin.fassmann@dlr.de

†Research Scientist, AIAA Member

‡Senior Scientist, Senior AIAA Member

§Head of Technical Acoustics Department, DLR Institute of Aerodynamics and Flow Technology, Senior AIAA Member

For an industrial application of acoustic optimization, numerical methods with short turnaround times are needed. Today's computational power allows a detailed and high resolution investigation of the edge noise problem with a variety of approaches. But full resolution of porous material with all its geometrical details at technical relevant Reynolds numbers still exceeds datum computer capability. Thus, a frequently used means of modeling porous material and multi-phase flow is the method of volume averaging, refer to 7–15. Breugem[16] uses the Volume Averaged Navier-Stokes (VANS) equations for his Computational Fluid Dynamics (CFD) simulations of a generic porous material. Liu and Vasilyev[17] use a Brinkman penalization technique for simulating flow and acoustics inside a porous material.

The present paper aims to extend the application of a hybrid CFD/CAA approach to include the effect of porous trailing-edge modification on broadband sound. The hybrid approach takes the time-averaged flow data and turbulence statistics from steady a Reynolds Averaged Navier-Stokes (RANS) simulation to model synthetic vortex sound sources and predict the aeroacoustic sound generation and radiation in space and time by means of Code for Computational Aeroacoustics (CAA). The CFD/CAA was applied in the past to different airframe[18–22] and jet noise[23–28] problems and was successfully used in the BANC III benchmark workshop[29,30] for the validation of NACA0012 trailing edge noise against measurements.

A set of linear propagation equations for porous regions is derived from VANS equations. They are referred to as Linear Perturbation Equations (LPE) to indicate that due to the additional inclusion of porosity factors, Darcy and Forchheimer terms, some essentials features of the Acoustic Perturbation Equations[31] (APE) are lost, i.e. the assumption of isentropic density and pressure fluctuations and resolution of purely irrotational velocity components in the absence of a vortex source term. However, the LPE provide a smooth transition between fluid regions, governed by the APE, and porous regions treated with the LPE.

Section II gives an overview about the applied method and presents the main details of the derivation of the LPE. In Section III, the set-up for two different CAA simulation sets is introduced. The first set-up is a generic test case. The propagation of acoustic waves in homogeneous porous material with spatially isotropic porosity properties is studied to verify the implementation. The second case is a feasibility test of the presented approach. A NACA0012 airfoil is equipped with a porous trailing edge. A close look on the special issues regarding the porous inlay is taken. Section IV discusses the CAA results for the two simulations set-ups. Finally, the acoustic benefit of the NACA0012 airfoil geometry with a permeable porous trailing edge treatment is compared to experimental data from Herr.[5]

II. Numerical Methods

In this section the numerical methods are presented, which are used to predict the aeroacoustic benefit of porous trailing edge treatment. First, Sec. II.A describes the method of volume averaging. Also, a set of independent variables is presented which enables a smooth transition between porous regions and free fluid. In Sec. II.B, the LPE are derived. The aeroacoustically relevant effects of the porosity are modeled by additional terms resulting from the averaging procedure. In Sec. II.C the used hybrid CFD/CAA approach is illustrated in more detail. Finally, in Sec.II.D the stochastic method to generate broadband vortex sound sources based on synthetic turbulence is outlined.

II.A. Volume averaging

The method of volume averaging is an important tool for multi-phase flows. Since the late 60th, a considerable amount of work has been dedicated to the development of volume averaged conservation and transport equations, see e.g. 7–15. The operation of volume averaging can be understood as spatial filtering of the flow variables. The superficial volume averaging is defined as follows:

$$\langle \rho \rangle^s (\boldsymbol{x}, t) := \frac{\int G(\boldsymbol{x} - \boldsymbol{x}', \Delta)\, \rho^*(\boldsymbol{x}', t) d^3x'}{\int G(\boldsymbol{x} - \boldsymbol{x}', \Delta)\, d^3x'}. \tag{1}$$

In this expression G denotes the spatial filter applied for the volume averaging procedure. The filter is centered at $\boldsymbol{x}$ and has a fixed extension defined by length scale Δ, i.e. it decays to zero for $|\boldsymbol{x} - \boldsymbol{x}'| >> \Delta$. For example, the filter could be chosen to be a Gaussian with standard deviation Δ.

The quantity ρ^* denotes the generalized density variable which is well defined in the entire volume, i.e. in the porous volume as well as in the solid phase of a porous material. It is given by

$$\rho^*(\boldsymbol{x}, t) = \rho(\boldsymbol{x}, t) H(f(\boldsymbol{x})). \tag{2}$$

Here, H denotes the Heaviside-function and $f(\boldsymbol{x})$ is a function defined to be $f < 0$ in the solid material and $f > 0$ in the fluid, i.e. $f = 0$ indicates the surface between solid and fluid in the porous medium, refer to Fig. 1. The gradient of $f(0)$ is normal to the interface surfaces. Without losing generality we can define the

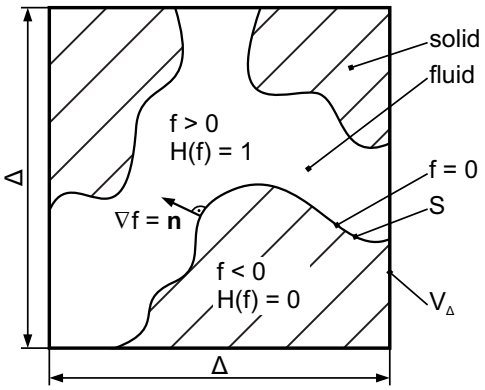

Figure 1. Schematic of porous material and definition of function $f(x)$.

scaling of f such that the gradient is the wall normal unity vector and points into the fluid, i.e. $\boldsymbol{\nabla} f = \boldsymbol{n}$. For further details regarding generalized variables and their application refer to Crighton.[32] The integrals (without explicitly specified bounds) are taken over the entire space. In general, the integral over the filter kernel defines a characteristic filter volume,

$$V_\Delta = \int G\left(\boldsymbol{x} - \boldsymbol{x}', \Delta\right) d^3x'. \tag{3}$$

The intrinsic averaged density is defined by

$$\langle\rho\rangle^i(\boldsymbol{x}, t) := \frac{\int G\left(\boldsymbol{x} - \boldsymbol{x}', \Delta\right) \rho^*(\boldsymbol{x}', t) d^3x'}{\int G\left(\boldsymbol{x} - \boldsymbol{x}', \Delta\right) H(f(\boldsymbol{x}')) d^3x'}. \tag{4}$$

A porosity factor $\bar{\phi}$ can be defined via

$$\bar{\phi} = \frac{\int G\left(\boldsymbol{x} - \boldsymbol{x}', \Delta\right) H(f(\boldsymbol{x}')) d^3x'}{\int G\left(\boldsymbol{x} - \boldsymbol{x}', \Delta\right) d^3x'}, \tag{5}$$

which, based on the definitions Eqs. (1) and (4) for intrinsic and superficial averaged quantities, yields the following generally valid relationship between both volume averaged quantities:

$$\langle\rho\rangle^s = \bar{\phi}\ \langle\rho\rangle^i. \tag{6}$$

It always is $0 \leq \bar{\phi} \leq 1$, where $\bar{\phi} = 1$ in free fluid and $\bar{\phi} = 0$ represents a solid body.

In the special case where the filter kernel is chosen to be a discontinuous top-hat function $G(\boldsymbol{x} - \boldsymbol{x}', \Delta) = g(x - x')g(y - y')g(z - z')$, $g(x)$ defined by

$$g(x) = 1 - H\left(|x| - \Delta/2\right), \tag{7}$$

the superficial averaged density reads

$$\langle\rho\rangle^s = \frac{1}{V_\Delta} \int\limits_{V_F} \rho d^3x'. \tag{8}$$

The top-hat function restricts the integration volume to a finite extension $V_\Delta = \Delta^3$ centered at the given position (window averaging). V_F is the fluid volume of the porous material inside the actual window; it satisfies $V_F = \bar{\phi}V$. The intrinsic volume averaged variable in this case becomes

$$\langle\rho\rangle^i = \frac{1}{V_F} \int\limits_{V_F} \rho d^3x'. \tag{9}$$

For a point inside the fluid phase the intrinsic density becomes in the limit $\Delta \to 0$ equal to the local density in the fluid, i.e.

$$\langle \rho \rangle^i (\boldsymbol{x}, t) \to \rho(\boldsymbol{x}, t) \quad \text{for} \quad \Delta \to 0. \tag{10}$$

In order to smooth out geometrical details of the porous medium, such that the volume averaged variables become continuous over the porous material, a length scale $\Delta > d_p$ must be used, where d_p denotes the characteristic pore size. In this case, the intrinsic volume averaged density has the same order of magnitude as a local density, it is, however, a quantity defined over the entire space, which moreover can be spatially differentiated if a continuous filter function G is applied. The superficial averaged density is smaller as defined by the porosity parameter $\bar{\phi}$. Hence, at interfaces between porous materials and free fluid the intrinsic density will only exhibit a gradual change over the interface, whereas the superficial averaged density will change rapidly over a scale Δ. Inside a homogeneous porous material, the explicit value of $\bar{\phi}$ will be independent for sufficient large Δ from the explicit chosen length scale in Eq. (5). However, at an interface between the porous medium and a free fluid, $\bar{\phi}$ will change gradually over a length Δ from its value in the porous medium to one inside the fluid phase.

Favre volume averaged velocities are defined via

$$[v_i] = \frac{\langle \rho v_i \rangle^{s,i}}{\langle \rho \rangle^{s,i}}. \tag{11}$$

As a consequence of definitions Eqs. (1) and (5) the definition is independent of whether superficial or intrinsic averaging is applied. To derive volume averaged perturbation equations, the Navier-Stokes equations in conservative notation are volume averaged assuming the application of a spatial differentiable filter $G(|\boldsymbol{x} - \boldsymbol{x}'|)$. In the fluid ($\bar{\Phi} = 1$) the resulting equations correspond to those used for Large Eddy Simulation (LES), i.e. they formally correspond to the Navier-Stokes equations for volume averaged variables plus some extra sub grid scale stress terms on the right-hand side. In this derivation step, commutation[a] of volume averaging and differentiation is applied, e.g. for the term ρv_i in the continuity equation it follows from the definition Eq. (1)

$$\left\langle \frac{\partial \rho v_i}{\partial x_i} \right\rangle^s = \frac{\partial}{\partial x_i} \left\{ \langle \rho \rangle^s [v_i] \right\}. \tag{12}$$

Independent variables For numerical stability reasons the independent perturbation variables finally used for the formulation of volume averaged LPE are selected based on the prerequisite to be (almost) continuous across an interface between fluid and the porous medium. This way, gradients that occur inevitably due to the sudden jump of porosity across the boundary can be lumped together in extra terms linear in the used independent variables which resemble a numerically resolved localized function with a distinct peak across the interface. If applied in conjunction with explicit time integration, these extra terms could trigger numerical instabilities. To circumvent this problem, their contribution can be treated implicitly in a mixed implicit-explicit time integration method (IMEX methods, refer to Refs. 33,34), whereas all spatial gradient terms occurring in the governing equations can be treated further on by means of explicit time integration. Since the extra terms are localized, i.e. proportional to the fluctuating variables and do not involve information from neighbor nodes of the computational mesh, implicit treatment in the framework of SDIRK methods[33] demands only for inversion of an $n \times n$ matrix (depending on the dimension n of the problem) composed out of steady mean-flow variables, which is computed and stored at the begin of an unsteady simulation cycle. Therefore, highly efficient treatment of these implicit gradient terms becomes feasible.

To discuss further the appropriate choice of independent variables, we consider a test set-up of an incompressible channel flow in which a zone of porosity is applied across the channel, refer to Fig. 2. For this case, the intrinsic density in the porous medium, where $0 < \bar{\phi} < 1$ holds, is a constant quantity, since

$$\langle \rho \rangle^i = \frac{\int GH\rho \mathrm{d}^3x}{\int GH \mathrm{d}^3x} = \frac{\rho \int GH \mathrm{d}^3x}{\int GH \mathrm{d}^3x} = \rho. \tag{13}$$

Mass conservation across the bulk and in the porosity implies $\rho u = \langle \rho \rangle^s [u] = \text{const}$. Using Eq. (13) and with the help of Eq. (6) this yields

$$u = \bar{\phi} [u]. \tag{14}$$

[a] see Appendix A

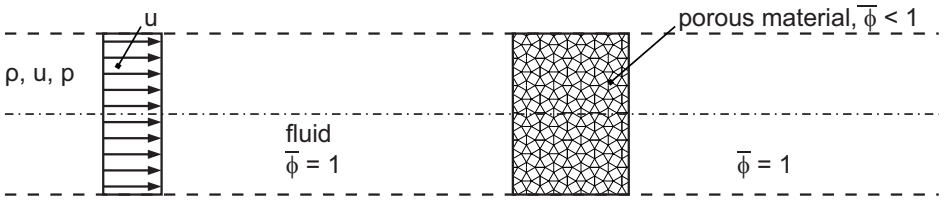

Figure 2. Sketch of channel flow with porous blocking.

Hence, to accomplish almost continuous variables across the fluid-porous interface, we introduce a new velocity variable defined by

$$\widehat{v_i} := \bar{\phi}\,[v_i]\,. \tag{15}$$

Furthermore, we chose the intrinsic volume-averaged fluctuating density $\langle\rho\rangle^i$ and the intrinsic volume-averaged fluctuating pressure $\langle p\rangle^i$ to close the set of independent variables. In the free fluid where $\phi = 1$,the perturbation variables correspond to the usual (APE) perturbation variables.

II.B. Volume averaged perturbation equations

For the derivation of volume averaged perturbation equations, the volume averaged pressure and density are decomposed into a mean, i.e. time-averaged, and a fluctuating part. Let ε indicate density or pressure, i.e. $\varepsilon \in \{\rho, p\}$, then the decomposition reads

$$\langle\varepsilon\rangle^{i,s} = \overline{\langle\varepsilon\rangle^{i,s}} + \langle\varepsilon\rangle^{i,s'}, \tag{16}$$

where the mean variable is defined by the time-average

$$\overline{a} = \lim_{\Delta t\to\infty} \int_{t_0}^{t_0+\Delta t} a\mathrm{d}t. \tag{17}$$

The Favre volume averaged velocity defined by Eq. (11) is decomposed into a Favre averaged mean-part plus a fluctuation, i.e.

$$[v_i] = \widetilde{[v_i]} + [v_i]''\,, \tag{18}$$

where

$$\widetilde{[v_i]} := \frac{\overline{\langle\rho\rangle^s\,[v_i]}}{\overline{\langle\rho\rangle^s}}, \tag{19}$$

with the bar indicating a time average, Eq. (17). It is easy to prove that Favre averaging applied to volume averaged quantities still satisfies the usual relations

$$\overline{\langle\rho\rangle^s\,[v_i]''} = 0 \tag{20}$$

and

$$\overline{\langle\rho\rangle^s\,[v_i]\,[v_j]} = \langle\rho\rangle^s\,\widetilde{[v_i]}\widetilde{[v_j]} + \overline{\langle\rho\rangle^s\,[v_i]''\,[v_j]''}. \tag{21}$$

Superficial volume averaging for density and pressure must be applied to the volume averaged Navier-Stokes equations to enable their reformulation in conservative notation that eventually can be transformed into a formulation based on primitive volume averaged variables, refer to Section II.A. Introduction of the variable decomposition and linearization allows deriving volume averaged perturbation equations in terms of independent variables $\left(\langle\rho\rangle^{s'}, [v_i]'', \langle p\rangle^{s'}\right)$. For the desired set of independent variables based on intrinsic volume averaged density and pressure as well as velocity defined by Eq. (15), in a final step the variables have to be substituted accordingly. To simplify the syntax, subsequently we will use a notation without additional brackets to indicate intrinsic volume-averaged quantities, e.g. ρ, ρ^0, and ρ' instead of $\langle\rho\rangle^i$, $\overline{\langle\rho\rangle^i}$, and $\langle\rho\rangle^{i'}$, respectively. Furthermore, a simplified notation is introduced for convenience by omitting the overbar on ϕ, i.e. $\overline{\phi} \to \phi$. Then the substitutions

$$\phi\rho' \to \langle\rho\rangle^{s'}, \quad \phi\rho^0 \to \overline{\langle\rho\rangle^s}, \quad \phi p' \to \langle p\rangle^{s'}, \quad p^0 \to \overline{\langle p\rangle^s} \tag{22}$$

have to be applied to eventually reformulate the perturbation equations in the desired set of variables. Proper velocities according to the definition Eq. (15) are obtained by the replacements

$$\frac{\hat{v}_i^0}{\phi} \rightarrow \widetilde{[v_i]}, \quad \frac{\hat{v}_i'}{\phi} \rightarrow [v_i]''. \tag{23}$$

The LPE are resulting from consequent application of the volume averaging procedure as outlined before derive as follows: The continuity equation of the LPE reads

$$\frac{\partial \rho'}{\partial t} + \phi^{-1}\left[\widehat{v}_i^0 \frac{\partial \rho'}{\partial x_i} + \widehat{v}_i' \frac{\partial \rho^0}{\partial x_i} + \rho^0 \frac{\partial \widehat{v}_i'}{\partial x_i} + \rho' \frac{\partial \widehat{v}_i^0}{\partial x_i}\right] = S_\rho. \tag{24}$$

The LPE momentum equations become

$$\begin{aligned} &\frac{\partial \widehat{v}_i'}{\partial t} + \phi^{-1}\frac{\partial \widehat{v}_k^0 \widehat{v}_k'}{\partial x_i} + \frac{\phi}{\rho^0}\left[\frac{\partial p'}{\partial x_i} - \frac{\rho'}{\rho^0}\frac{\partial p^0}{\partial x_i}\right] \\ &\quad + \underbrace{\frac{\phi\nu}{\kappa}\delta_{ij}\widehat{v}_j'}_{\text{Darcy term}} + \underbrace{\frac{\phi c_\mathrm{F}}{\sqrt{\kappa}}\sqrt{\widehat{v}_k^0 \widehat{v}_k^0}\left[e_i^0 e_j^0 + \delta_{ij}\right]\widehat{v}_j'}_{\text{Forchheimer term}} \\ &\quad + \underbrace{\left(\widehat{v}_i^0 \frac{\partial \phi^{-1}}{\partial x_j} + \delta_{ij}\widehat{v}_k^0 \frac{\partial \phi^{-1}}{\partial x_k}\right)\widehat{v}_j' + \frac{\phi^2}{\rho^0}\left(\frac{\rho' p^0}{\rho^0} - p'\right)\frac{\partial \phi^{-1}}{\partial x_i}}_{\text{gradient model terms}} \\ &\quad = S_{v,i}, \end{aligned} \tag{25}$$

where ν denotes the kinetic viscosity, and the symbol κ identifies the permeability. In the free fluid, the reciprocal of the permeability is $\kappa^{-1} = 0$ and in the porous material it is $\kappa^{-1} \gg 1$, while for a solid wall $\kappa^{-1} \rightarrow \infty$. Further, the Forchheimer coefficient is represented by c_F, δ_{ij} means the Kronecker delta and e_i^0 indicates the direction of the time averaged mean flow velocity. The inclusion of the Darcy and Forchheimer terms in the governing equations is shown in more detail in Appendix A.

The energy equation in terms of pressure is

$$\frac{\partial p'}{\partial t} + \phi^{-1}\left(\widehat{v}_i^0 \frac{\partial p'}{\partial x_i} + \widehat{v}_i' \frac{\partial p^0}{\partial x_i}\right) + \gamma\phi^{-1}\left(p^0 \frac{\partial \widehat{v}_i'}{\partial x_i} + p' \frac{\partial \widehat{v}_i^0}{\partial x_i}\right) + \underbrace{(\gamma - 1)\left(p^0 \widehat{v}_i' + p' \widehat{v}_i^0\right)\frac{\partial \phi^{-1}}{\partial x_i}}_{\text{gradient model terms}} = S_p, \tag{26}$$

where $\gamma = 1.4$ is the isentropic exponent of ambient air. The right-hand source terms are indicated by $S_{\rho,v,p}$. Please note that the continuity equation and the energy equation of the LPE equal those of the volume averaged Linearized Euler Equations (LEE). Thus, the set of LPE differs from the APE except for the right-hand side source term in the momentum equation. Further, the LPE resolve the entropy mode but, unlike the LEE, do not contain the vorticity mode.

II.B.1. Modified Wave Equation

For a medium at rest, the theoretical damping envelope of a porous material can be derived from the damped 1-D wave equation that results from Eqs. (26) and (25). Based on some prerequisites $v_i^0 = 0$, $p^0 = \text{const.}$, $\rho^0 = \text{const.}$, $\phi = \text{const.}$, the pressure and momentum equation of the acoustic propagation equations (LEE, LPE) reduce to

$$\frac{\partial v_i'}{\partial t} + \frac{\phi}{\rho^0}\frac{\partial p'}{\partial x_i} + D_{ij} v_j' = 0 \tag{27}$$

$$\frac{\partial p'}{\partial t} + \frac{\gamma p^0}{\phi}\frac{\partial v_i'}{\partial x_i} = 0. \tag{28}$$

For a material with isotropic acoustic properties it is $D_{ij} v_j' = D v_i' = \phi\,\nu/\kappa\, v_i'$. Introducing the acoustic potential

$$v_i' = \frac{\partial \varphi}{\partial x_i}, \tag{29}$$

the system reads

$$\frac{\partial^2\varphi}{\partial t\partial x_i}+\frac{\phi}{\rho^0}\frac{\partial p'}{\partial x_i}+D\frac{\partial\varphi}{\partial x_i}=0 \tag{30}$$

$$\frac{\partial p'}{\partial t}=-\frac{\gamma p^0}{\phi}\frac{\partial^2\varphi}{\partial x_i^2}. \tag{31}$$

Now, the time derivative of Eq. (30) and the spatial derivative of Eq. (31) with respect to x_i are taken. Using $c_0^2=\gamma p^0/\rho^0$, a wave equation for the acoustic potential is obtained:

$$\frac{\partial}{\partial x_i}\left(\frac{\partial^2\varphi}{\partial t^2}-c_0^2\frac{\partial^2\varphi}{\partial x_i^2}\right)+D\frac{\partial^2\varphi}{\partial t\partial x_i}=0. \tag{32}$$

Note, the first term in brackets alone represents the homogeneous wave equation, while the additional term represents the effect of the porosity. Finally, the 1-D wave equation reads

$$\frac{\partial^2\varphi}{\partial t^2}-c_0^2\frac{\partial^2\varphi}{\partial x^2}+D\frac{\partial\varphi}{\partial t}=0, \tag{33}$$

what leads to

$$p'=-\frac{\rho^0}{\phi}\left(\frac{\partial\varphi}{\partial t}+D\varphi\right). \tag{34}$$

Considering harmonic signals with $\hat{\varphi}(x,t)=\hat{A}\exp\left(i\left(\omega t-kx\right)\right)$, the corresponding pressure fluctuations can be expressed as

$$\hat{p}=-\frac{\rho^0}{\phi}\left[\left(i\omega+D\right)\hat{\varphi}\right] \quad . \tag{35}$$

Furthermore, introducing the harmonic ansatz into the wave-equations yields the dispersion relation

$$-\omega^2+k^2c_0^2+i\omega D=0. \tag{36}$$

By means of the dispersion relation, the wave number k may be written as a function of angular frequency ω yielding the damped wave results

$$\hat{\varphi}=\hat{A}\exp\left(i\omega\left(t-\frac{1}{c_0}\sqrt{\frac{1}{2}\left[\sqrt{\frac{D^2}{\omega^2}+1}+1\right]}\,x\right)\right)\exp\left(-\frac{\omega}{c_0}\sqrt{\frac{1}{2}\left[\sqrt{\frac{D^2}{\omega^2}+1}-1\right]}\,x\right) \tag{37}$$

The damping can be expressed by the ratio of the local root mean square value $\tilde{p}(x)$ of the sound pressure $p'(x,t)$ to its value $\tilde{p}(0)$ at the origin $x=0$, i.e. $\tilde{p}^2=\overline{(p')^2}$. Considering a homogeneous, isotropic porosity, the damping envelope with respect to x results from Eqs. (34) and (37):

$$\frac{\tilde{p}(x)}{\tilde{p}(0)}=\exp\left(-\frac{\omega}{c_0}\sqrt{\frac{1}{2}\left[\sqrt{\frac{(\phi\,\nu\,\kappa^{-1})^2}{\omega^2}+1}-1\right]}\,x\right). \tag{38}$$

II.C. Hybrid CFD/CAA approach

The DLR-PIANO-CAA-Code[35] is applied in a hybrid two-step procedure. The first step rests on a CFD simulation of the time-averaged turbulent flow around the airfoil. In the second CAA step, time dependent linear propagation equations are solved on structured multi-block (SMB) meshes to compute the sound field. The resulting acoustic quantities, i.e. the spatially and time-resolved sound pressure, the acoustic particle velocity and the sound intensity can be evaluated at user-chosen microphone positions. All acoustic information may be collected on Ffowcks-Williams-Hawkings-Surfaces to be propagated to the far field during a separate post processing.

On the right-hand side of the linear propagation equations, sound sources must be explicitly imposed. For the computation of trailing edge noise, a vorticity based sound source is applied. A synthetic turbulence method provides fluctuating vorticity according to the turbulence statistics of the RANS solution. The Fast

Random Particle-Mesh Method (FRPM)[22,36,37] realizes time-dependent fluctuations from time-averaged turbulence statistics. The method generates Gaussian correlated synthetic turbulence of local integral length scale $\Lambda = c_\Lambda \sqrt{k}/\omega$ (with $c_\Lambda = c_l/C_\mu$ and $c_l \simeq 0.5$, $C_\mu = 0.09$, respectively) and variance proportional to the turbulence kinetic energy distribution, refer to Section II.D for further details.

Fig. 3 gives a general overview about the approach. The steady time-averaged RANS flow provides

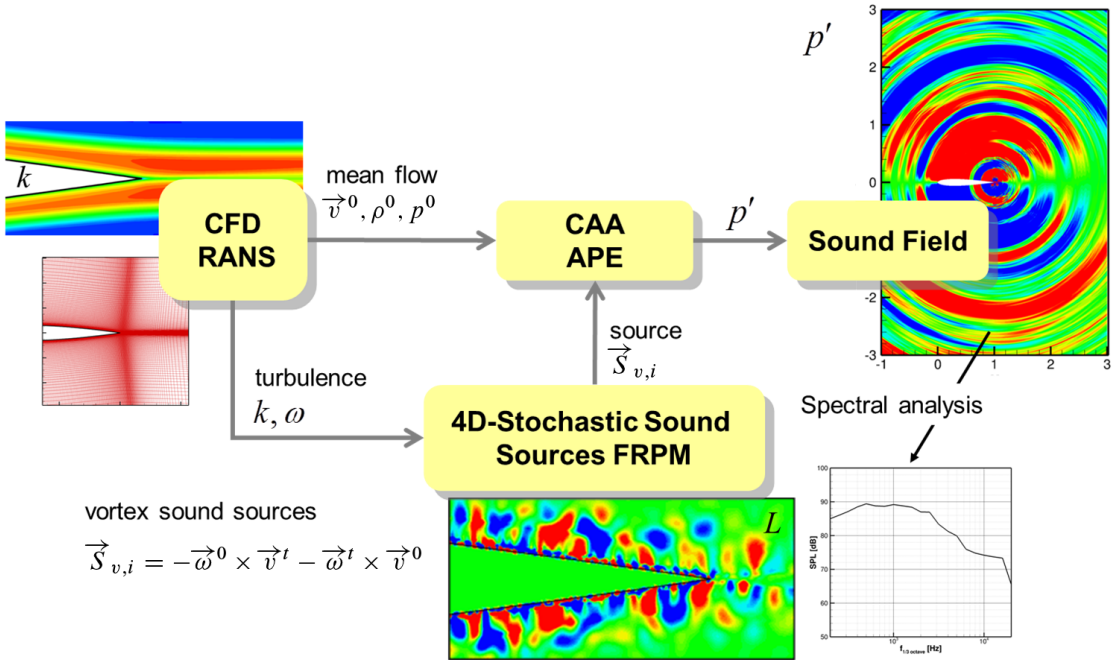

Figure 3. Schematic of CAA prediction method of DLR based on a two-step hybrid method using a steady RANS CFD step, followed by a CAA step solving Acoustic Perturbation Equations (APE) in the free field on structured multi block (SMB) meshes; the generation of fluctuating turbulent sound sources is realized with the 4-D FRPM synthetic turbulence method.

the mean-flow over which the time dependent aeroacoustic simulation is carried out. Furthermore, the turbulence statistics provided by RANS is utilized to generate the unsteady vortex sound sources that drive the governing equations.

In free field, this turbulence is coupled with the CAA solver, which is based on the 4th order accurate DRP scheme proposed by Tam & Webb.[38] The synthetic turbulence in conjunction with the RANS mean-flow defines the right-hand side fluctuating source terms of the APE, which are a modification of the LEE so that vorticity or entropy convection is entirely prescribed by the source term whereas acoustic generation and radiation is simulated dynamically. The APE realize a solution to the wave operator of irrotational flow. Together with proper right-hand side volume sources this becomes an acoustic analogy based on that wave operator. The source term mainly acts as a vorticity production term. Sound due to the interaction of vorticity with the trailing-edge is generated as part of the CAA simulation step. These vortex dynamics are dominated by the linear contributions to the source terms. Within the porous regions, the LPE are excited by the same right-hand side source term depending on the local kinetic energy of the turbulence. Like the LEE, the LPE do not suppress the entropy modes of the solution. Non-linear contributions are neglected for LPE and APE.

II.D. Stochastical Broadband Sources

For the simulation of broadband sound generation the perturbation equations are excited by stochastically generated right-hand side sources. As the dominating source of vortex sound the fluctuating (linearized) Lamb vector is modeled on the right-hand side of the momentum equation, i.e.

$$S_{v,i} = -\epsilon_{ijk}\omega_j^0 v_k^t - \epsilon_{ijk}\omega_j^t v_k^0, \tag{39}$$

where ϵ_{ijk} is the Levi-Civita-symbol. Altogether the system Eqs. (24) to (26) with source (39) constitutes an acoustic analogy based on the wave-operator of irrotational flow, taking into account only the vortex

sound source contributions. For the CAA simulations the steady RANS solution is used to prescribe the mean-flow. The mean flow vorticity $\omega_i^0 = \epsilon_{ijk}\partial v_k^0/\partial x_j$ needed to specify the source is computed from the RANS mean-flow velocity. The fluctuating turbulent velocities v_i^t are modeled stochastically with the FRPM method, refer to the next section, from which the fluctuating vorticity is derived as $\omega_i^t = \epsilon_{ijk}\partial v_k^t/\partial x_j$.

The LPE and APE suppress the vorticity mode otherwise present in the LEE and as such convective and absolute hydrodynamic instabilities that can plague the LEE are removed, see.[31] Convecting vorticity can be present in the LPE/APE perturbation velocity, but is entirely prescribed by the right-hand side source term. To be precise, vortex sound sources serve on the one hand as a direct sound source, describing the sound generation in free turbulence. On the other hand it acts as a pure vorticity source in the perturbation equations. Airframe noise generation is due to the interaction of unsteady convecting turbulence (vorticity) with sharp edges. In previous work with PIANO it was extensively demonstrated, e.g. by injecting test vortices into the LEE, that the linear CAA equations are capable of predicting the essential noise sound generation at trailing edges, i.e. the physical conversion process of the vorticity mode into an acoustic mode that take place in the vicinity of geometrical inhomogeneities such as sharp trailing edges.[39]

III. Computational Set-up

The implementation of the acoustic porosity model will be checked by a two-stage procedure. First, the code is verified comparing the acoustic solution with the analytical solution of the 1-D wave equation. Second, a feasibility test of the implementation will follow. The numerical results of 2-D simulations of an airfoil with porous trailing edge treatment will be compared to the acoustic benefit measured at a 2-D wing with the same treatment. The current section will give an insight in the numerical set-up of the two studies.

III.A. Verification Set-up

The proper implementation of the extra terms modeling the effect of porosity will be proven by comparison of a simple test case with the related analytical solution. The wave propagation within a quiescent medium is considered. The solutions of the reference free medium as well as two different isotropic homogeneous permeable porous materials are studied. One of these is a generic material with artificially chosen porosity parameters. The other material is a realistic porous aluminum, referred to as pAl80, with parameters deduced from measurements.

The 2-D computational domain extends from $x/l_{\text{ref}} = 0$ to $x/l_{\text{ref}} = 2$ and from $y/l_{\text{ref}} = -0.1$ to $y/l_{\text{ref}} = 0.1$. The fluid phase is ambient air considered as an ideal gas with properties $c_0 = 343\,\text{m/s}$, $p^0 = 1.01325 \cdot 10^5\,\text{Pa}$ and $\rho^0 = 1.205\,\text{kg/m}^3$. The grid is designed to resolve frequencies up to $f = 20\,\text{kHz}$. No additional background damping was used. The quiescent medium is excited by mono-frequent incoming plane waves with different frequencies. They are specified at the left boundary through a Thompson boundary condition.[40,41] In Fig. 4, a snap shot of the acoustic response is shown for a harmonic signal at 2 kHz. The signals for the quantitative evaluation are picked from a horizontal line centered in the computational

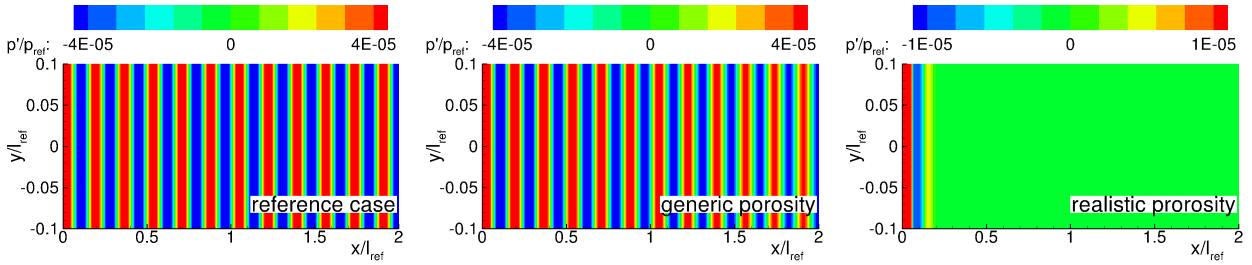

Figure 4. Snapshot of the acoustic response to harmonic plane waves at 2 kHz for three different isotropic materials; (left) free medium as a reference, (middle) generic porosity and (right) realistic porosity. The reference pressure is $p_{\text{ref}} = \rho^0 c_0^2$ and the reference length is $l_{\text{ref}} = 1\,\text{m}$.

zone.

III.B. Use Case

Hybrid RANS based CFD/CAA prediction of aeroacoustic sound generation demands for a suitable solution of the flow that also takes into account the effect of porosity on the mean flow and turbulence statistics.

This solution was provided by Institute of Fluid Mechanics of Technische Universität Braunschweig, using a VANS model for simulating porous regions of a computational area. This was added to the DLR in-house CFD solver TAU by Mößner.[42] With this model, 2-D RANS simulations of the flow field around and through a clean NACA0012 airfoil with a realistic porosity were performed. The porosity was located at the trailing edge, covering the last 11.25% of the airfoil. The numerical set-up is depicted in Fig. 5.

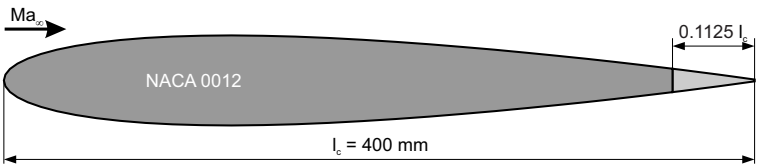

Figure 5. Set up of the porous trailing edge at a NACA0012 geometry at $\mathbf{Ma}_\infty \approx 0.12$, $\mathbf{Re}_\infty = 1.0{\cdot}10^6$ and $\mathbf{Ma}_\infty \approx 0.15$, $\mathbf{Re}_\infty = 1.3{\cdot}10^6$ at an angle of attack of $\alpha = 0\,\mathrm{deg}$.

For saving computational time, the 2-D CAA grid has a smaller extension than the CFD. The 2-D computational domain extends from $x/l_c = -2$ to $x/l_c = 4$ and from $y/l_c = -3$ to $y/l_c = 3$. The structured CAA mesh of the solid reference case consists of $\approx 1.5{\cdot}10^6$ grid points, distributed to 69 blocks. The mesh is designed for a field frequency resolution of 10 kHz using 7 points per wavelength resolution. The smallest mesh cells are located in the FRPM area covered by the source region. For the porous trailing-edge use cases, the same grid was used, except for additional $7.5 \cdot 10^3$ grid points within the porous region of the trailing edge, divided into 9 additional blocks. Fig. 6 shows the grid, normalized by the chord length l_c, in an overview and the magnification of the porous resolved region. The minimal explicit time step allowed is

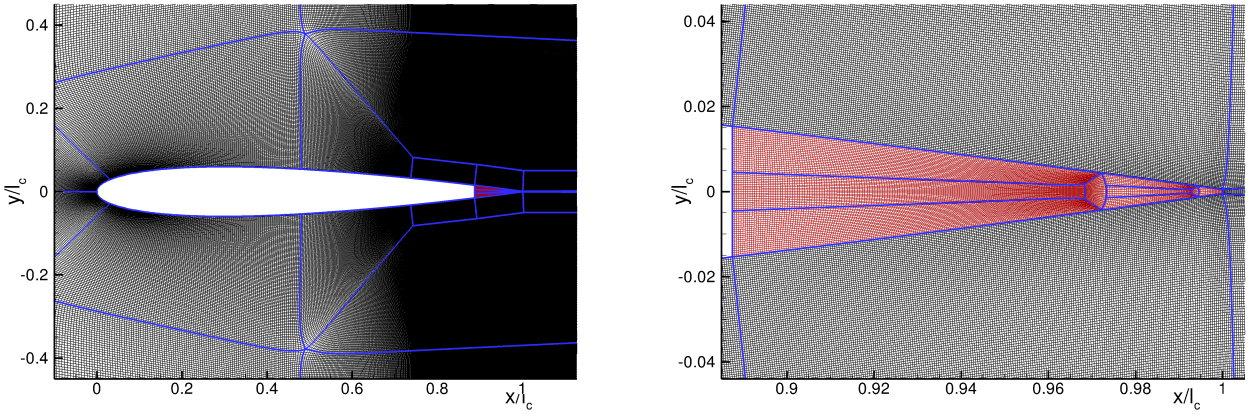

Figure 6. (left) computational mesh for CAA simulations of the porous 2-D NACA0012 airfoil; (right) detailed view of the porous region (red mesh) at the trailing edge.

$\Delta t \approx 1.3 \cdot 10^{-7}\,\mathrm{s}$. But, to prevent any numerical instability caused by the porosity model, a smaller time step of $\Delta t \approx 1.2 \cdot 10^{-7}\,\mathrm{s}$ was used. This leads to a roughly 10% higher computational time in total. The computation of $1.25{\cdot}10^6$ time steps was performed within about 90 hours on a state-of-the-art cluster system, using 12 CPUs in parallel. The total real time sampling length is $t \approx 0.15\,\mathrm{s}$.

In both cases, the solid reference case and the case with modified trailing edge with porosity, the acoustic field in the outer region is computed by the APE. In the inner region inside of the trailing edge, the LPE predict the acoustics. These equations use the spatial distribution of all relevant material parameters as the porosity ϕ, its reciprocal ϕ^{-1}, the reciprocal of the permeability κ^{-1} and the Forchheimer factor c_F as additional input. To prevent jumps of the porous field parameters, they are smoothed out at the interfaces to both regular computational zones and interfaces from porous regions to solid walls. The porosity variables are adjusted during preprocessing. The contour plot of the porosity ϕ in the vicinity of the trailing edge is depicted in Fig. 7. The complete set of variables is given in a horizontal and a vertical profile. The nominal values of the porosity parameters for the free air and the porous material are given, as well.

The simulation procedure concerning the excitation of the acoustics by the FRPM-method is following Rautmann et al.[30]

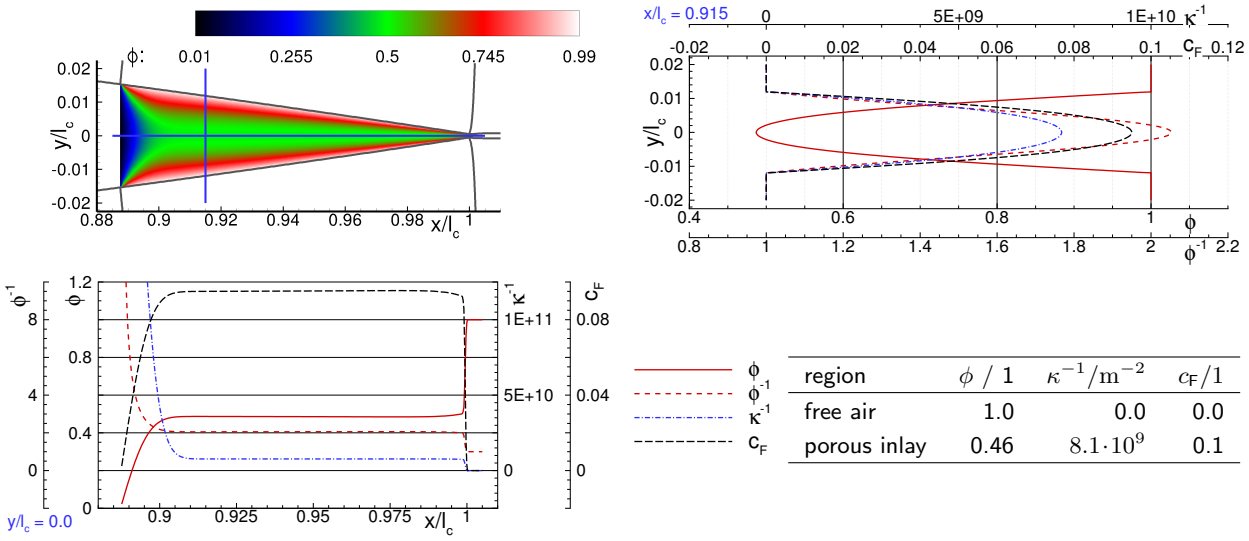

Figure 7. Spatial distribution of the material parameters, i.e. the porosity ϕ, its reciprocal ϕ^{-1}, the reciprocal of the permeability κ^{-1} and the Forchheimer factor c_F. Top left: Contour plot of the porosity at the trailing edge of the airfoil. Top right: Local distribution of the quantities at $x/l_c = 0.915$ as a function of y. Bottom left: Local distribution of the quantities at $y/l_c = 0.0$ as a function of x. Bottom right: Nominal material parameters for porous aluminum with a pore size of $80\,\mu$m to $110\,\mu$m.

IV. Simulation Results

This section presents the results of the numerical simulation of the two test cases. First, the agreement between the analytical damping behavior and the computational results for the generic plane wave problem is discussed. Next, the sound reducing benefit of the porous treatment of a NACA0012 trailing edge is evaluated.

IV.A. Verification Set-up

For a medium at rest, the theoretical damping envelope can be derived from the 1-D wave equation, see Eq. (38). In Fig. 8, the results from simulation are juxtaposed to the theoretical decay envelope. The acoustic signal from CAA matches the theoretical damping envelope. The damping envelope can be reduced to the expression

$$\frac{\tilde{p}(x)}{\tilde{p}(0)} =: \exp(-\lambda^{(\mathrm{D,sim})} x) \quad . \tag{40}$$

While the exponent (D) denotes the analytical damping behavior, the exponent (sim) indicates the damping behavior predicted by the simulation. Further, it is L_p the sound pressure level of $\tilde{p}$, namely

$$L_\mathrm{p}^{(\mathrm{D,sim})}(x) = 20 \log\left(\frac{\tilde{p}(x)}{\tilde{p}_\mathrm{max}}\right) = \frac{-20}{\ln(10)} \lambda^{(\mathrm{D,sim})} x \quad . \tag{41}$$

Finally, the degree of agreement between the analytical result and the computation can be expressed by

$$L_\mathrm{p}^{(\mathrm{sim})} = f(\lambda^{(\mathrm{D})} x) \quad . \tag{42}$$

The plot of the level decay of the rms-values within the computational domain is shown in Fig. 9. Normalized by the individual expected theoretical damping envelope $\lambda^{(\mathrm{D})}$, the contrasting material parameters show the same reduction of the local sound pressure levels. The prediction accuracy is comparable for a wide frequency range. The implementation of the porous model seems properly verified.

IV.B. Use Case

A feasibility study of the presented simulation method is performed by predicting the aeroacoustic benefit of a porous trailing edge concerning turbulent boundary layer trailing edge noise. Therefore, the broadband

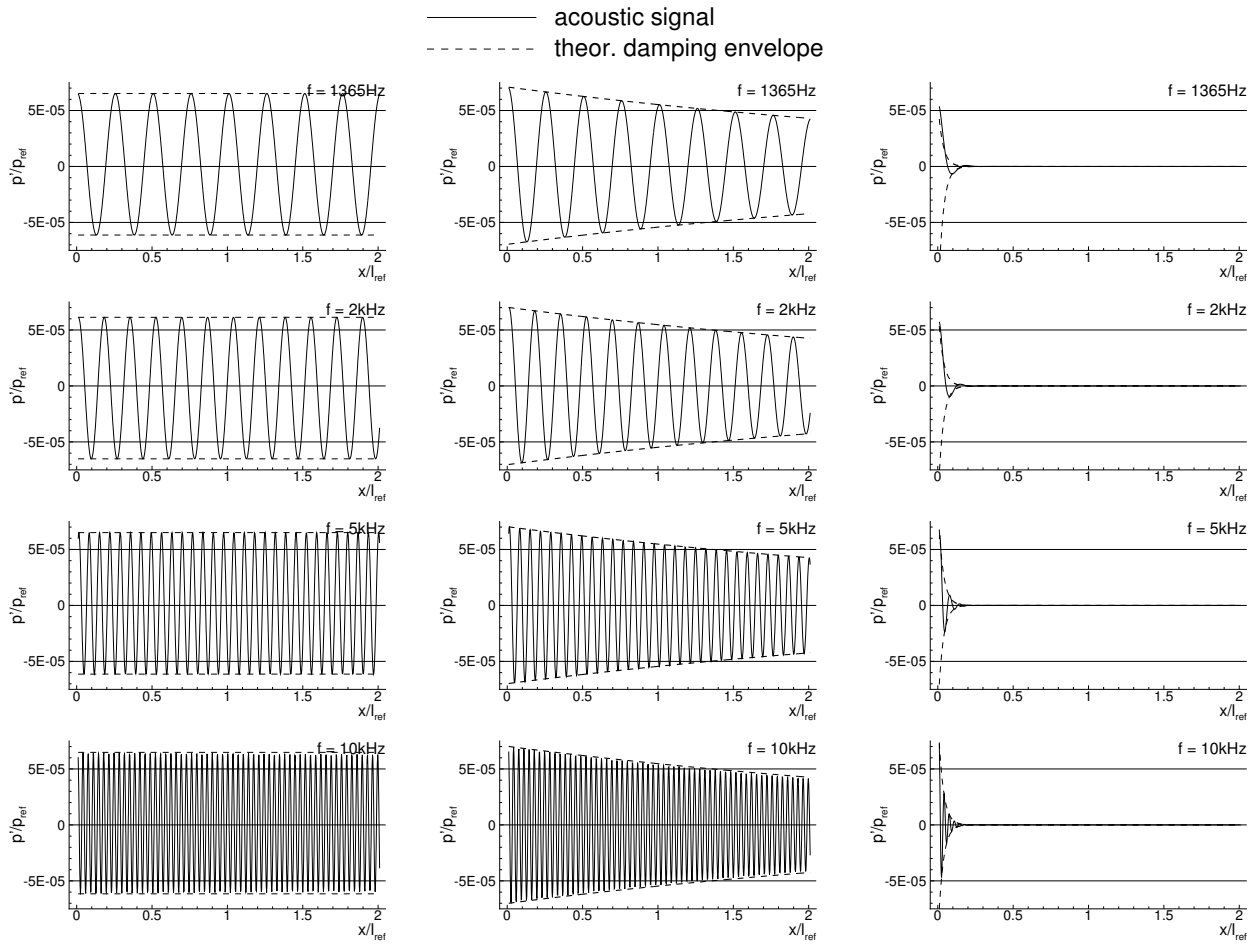

reference case:
$\phi = 1.0, \frac{\nu}{\kappa} = 0.0\,\frac{1}{\mathrm{s}}$

generic porosity:
$\phi = 0.8, \frac{\nu}{\kappa} = 214\,\frac{1}{\mathrm{s}}$

realistic porosity:
$\phi = 0.46, \frac{\nu}{\kappa} = 122{\cdot}10^3\,\frac{1}{\mathrm{s}}$

Figure 8. Comparison of CAA results of the Linear Perturbation Equations (LPE) and theoretical damping envelope of the 1-D wave equation in a medium at rest from Eq. (38) for isotropic porosity.

sound field of a NACA0012 geometry with a solid and a porous trailing edge at $\alpha = 0\,\mathrm{deg}$ angle of attack is computed. The results are then compared to the experimental results of Herr.[5] There, a reduction of about 6 dB was reported for a slit trailing edge compared to the solid reference case. In this section, the simulation results will be presented.

The two snap shots of the CAA simulations a solid and a porous trailing edge in Fig. 10 show a noticeable difference in the levels of the acoustic pressure. Fig. 10 confirms the qualitative impression from Fig. 11. The directivities of the investigated velocity case show a reduction of the limited overall sound pressure level (OASPL) for the frequency range of $f = 125\,\mathrm{Hz} \ldots 5\,\mathrm{kHz}$. At angles from $\theta = 195\,\mathrm{deg} \ldots 270\,\mathrm{deg}$, the OASPL is reduced by roughly 6 dB. Further, the typical cardioidic directivity is distorted if the trailing edge was treated with porosity. The numerical study then shows an augmentation of the levels in upstream and downstream direction. One can assume the onset of the porous inlay at the upper and the lower side of the airfoil to be two separate edges generating noise. This would evoke a superposed sound source which might have a streamwise oriented dipole characteristic. As a consequence, sound is emitted to both upstream and downstream direction.

Fig. 12 shows the frequency spectrum of at the microphone position 270 deg. The spectra of simulation and measurement show a good agreement for the solid reference. The location of the maximum and the general decrease of the spectra lie within the margin of errors of the measurement. The results of the porous simulation show a noise reduction of the order of 3 dB to 9 dB in the frequency range from $f = 125\,\mathrm{Hz}$ to $f = 5\,\mathrm{kHz}$. This first result successfully demonstrates the numerical prediction of trailing edge noise reduction by application of porous material of the same magnitude as observed in experiments.

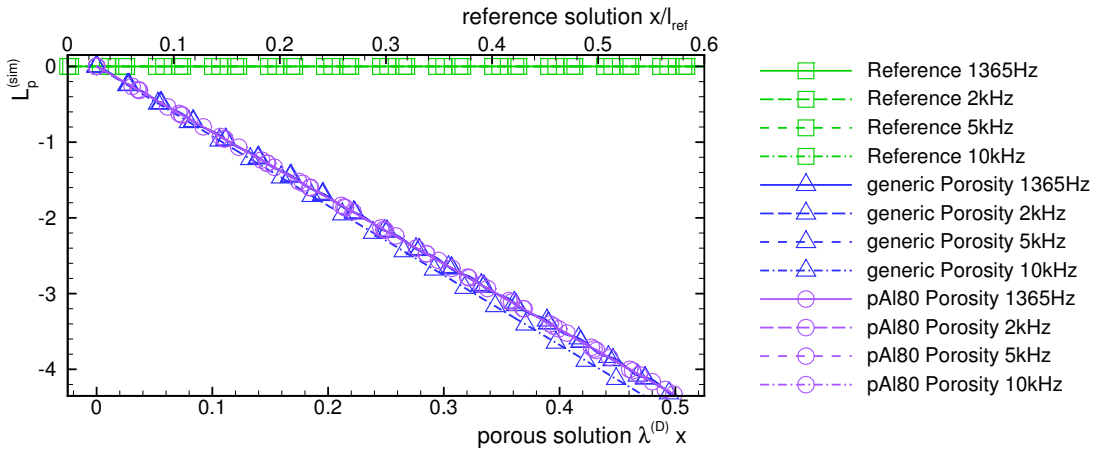

Figure 9. Comparison of CAA results of Linear Perturbation Equations (LPE) and theoretical damping envelope of the 1-D wave equation in a medium at rest from Eq. (40) for isotropic porosity. For the reference case, the computational prediction is given without relation to the theoretical damping coefficient, what is $\lambda^{(D)} = 0$ for the free medium.

V. Summary

The paper presents a method predicting the fluctuating sound field in the presence of a permeable porous material. An extended set of governing equations is developed by volume averaging the Navier-Stokes equations. This formal procedure leads to additional terms in the momentum equation and the energy equation. All terms explicitly representing viscosity, heat conduction and sub-filter stresses are omitted in the context of sound propagation. The remaining terms are modeled by the Darcy and Forchheimer terms at the left-hand side of the momentum equation. These terms model the effect of the complex structure inside of the porous material in terms of additional forces like drag and viscosity. Based on the physical idea of a finite averaging volume, continuous flow quantities are provided. The resulting set of governing equations is reformulated with intrinsically averaged primitive variables density and pressure. Further, a new Favre averaged velocity is defined, which is steady across the edge of free fluid and porous material. In the last step of the derivation, a decomposition of all variables into a steady meanflow and fluctuation is performed. Linearization of the fluctuating part leads to a new set of propagation equations, referred to as Linear Perturbation Equations (LPE). The LPE model the acoustic effect of porosity attached to structural parts e.g. of an airfoil. The LPE are comparable to the Linearize Euler Equations (LEE). Like them, the LPE do not suppress the entropy modes of the solution, but like the Acoustic Perturbation Equations (APE), the new set of equations does not contain the vorticity mode. This part of the solution is imposed by a right-hand side source term in the momentum equations. These sources must additionally be modeled by e.g. the Fast Random Particle Mesh Method (FRPM Method) or analytic sources. This way, a continuous transition from forced APE to the porous regions is accomplished.

Interaction of both, flow and acoustics with porous parts in the flow field must be correctly predicted to reproduce the noise reducing effect of porosity proven by experiments by Herr et al.[6] Therefore, verification and validation of the equations and their implementation is necessary. As a first step, a modified 1-D wave equation for a homogeneous porous material and stagnant fluid is used to proof the correct damping effect of the implementation. The results of the simulations agree with the analytical results. Next, the new functionality is applied to a 2-D NACA0012 airfoil geometry. The resulting edge noise reduction by porous treatment of the trailing edge is compared to experimental data from wind tunnel tests in the Aeroacoustic Wind tunnel Braunschweig (AWB). There, a good agreement between measurement and computational data is found for the solid reference case. The results of the porous use case show a broadband reduction in level for the frequency range of $f = 125\,\mathrm{Hz}$ to $5\,\mathrm{kHz}$.

VI. Outlook

For the DLR-F16 airfoil geometry, there exists a large database of aeroacoustic measurements with different trailing edge treatment by Herr et al.[6] The authors report of a maximal sound reduction of 6 dB to 8 dB. The next step of the validation process will be the simulation of the same setup in 2D. Additionally, the

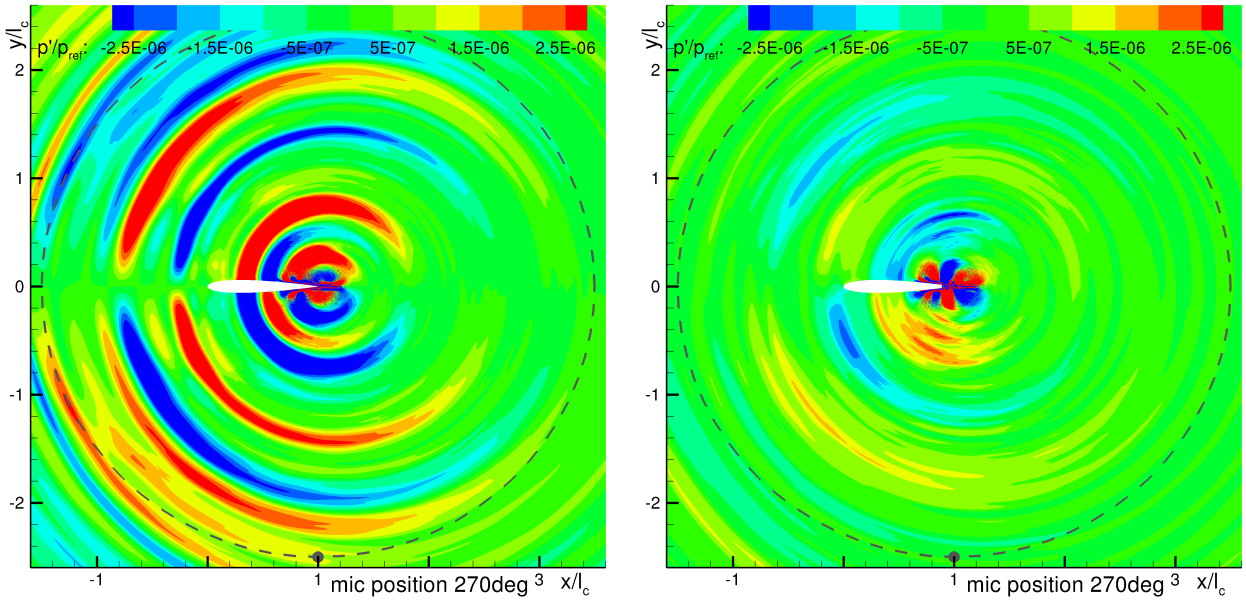

Figure 10. Snapshot of the sound field caused by turbulent boundary layer trailing edge noise at a NACA0012 airfoil without (left) and with (right) porous treatment. The dashed circle correlates with the distance of the 360 microphones. The highlighted microphone corresponds to the microphone position of the experiments at 270 deg.[6] The angle of attack is $\alpha = 0\,\mathrm{deg}$.

Mach number scaling law will be checked. Further validation of the implementation will be carried out with acoustic measurements from an impedance tube. In this test series, the same materials were acoustically characterized as Herr et al.[6] used them for their application at the trailing edge.

Further, the numerical properties of the new method will be identified. One drawback of the actual implementation is the need for a smaller timestep if porous treatment is applied with explicit time integration. To overcome this, an IMEX approach is planned to sbe implemented as proposed by Ascher[33] and Boscarino.[34] By this, the 2-D porous model can be applied without time step limitation.

Beyond porous material with isotropic properties, the presented porosity model can be extended to anisotropic materials. This seems to be useful optimizing porous materials for certain applications.

VII. Acknowledgement

Financial support has been provided by the German Research Foundation (Deutsche Forschungsgemeinschaft, DFG) in the framework of the Sonderforschungsbereich 880. Computational resources have been provided by German Aerospace Center (Deutsches Zentrum für Luft- und Raumfahrt e.V., DLR), Institute of Aerodynamics and Flow Technology.

The authors thank Michael Mößner from Technische Universität Braunschweig for providing the CFD of the porous F16 airfoil and Nicolas Lippitz also from Technische Universität Braunschweig for providing the measurement results of the impedance tube.

References

[1]Radespiel, R. and Heinze, W., "SFB 880 – Fundamentals of High-Lift for Future Commercial Aircraft," *Deutscher Luft- und Raumfahrtkongress 2013*, edited by D. G. f. L.-u. R. DGLR, Dt. Ges. für Luft- u. Raumfahrt, 2013.

[2]Hayden, R. E., "Reduction of Noise from Airfoils and Propulsive Lift Systems using variable Impedance Systems: Palo Alto, CA, July 20 - 23, 1976," *3rd AIAA Aeroacoustics Conference*, edited by American Institute of Aeronautics and Astronautics, American Institute of Aeronautics and Astronautics, 1976.

[3]Howe, M. S., "On the Added Mass of a Perforated Shell, with Application to the Generation of Aerodynamic Sound by a Perforated Trailing Edge," *Proceedings of the Royal Society of London. A. Mathematical and Physical Sciences*, Vol. 365, No. 1721, 1979, pp. 209–233.

[4]Hayden, R. E. and Chanaud R.C., "Foil Structures with Reduced Sound," 1974.

[5]Herr, M., "Design Criteria for Low-Noise Trailing-Edges," AIAA Paper 2007-3470, 2007.

[6]Herr, M., Rossignol, K.-S., Delfs, J. W., Mößner, M., and Lippitz, N., "Specification of Porous Materials for Low-Noise

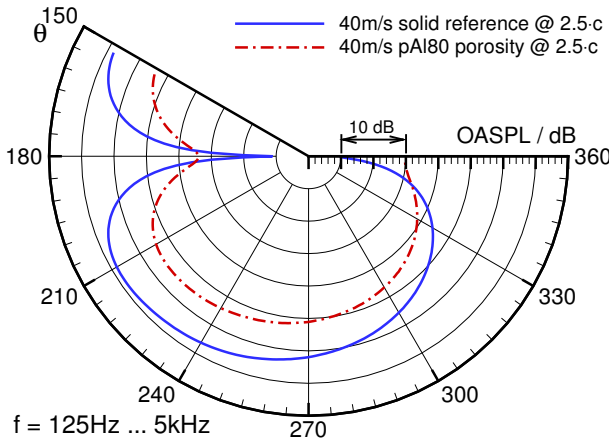

Figure 11. Directivity of the turbulent boundary layer trailing edge noise in terms of the limited overall sound pressure level (OASPL) in the range of $f = 125\,\mathrm{Hz} \ldots 5\,\mathrm{kHz}$. The porous trailing edge treatment effects a nearly omni-directional reduction of the OASPL of $6\,\mathrm{dB} \ldots 8\,\mathrm{dB}$.

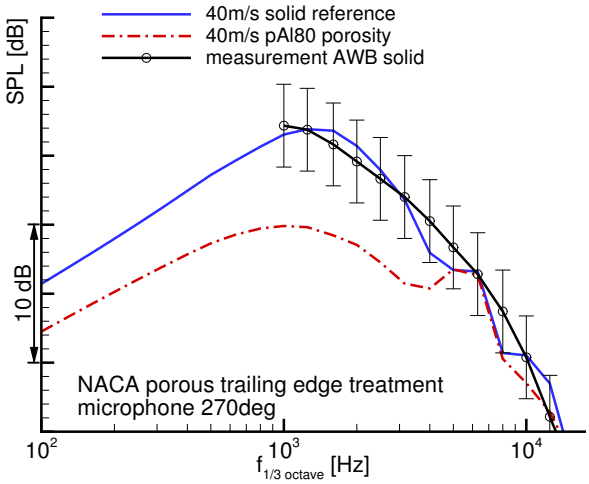

Figure 12. Spectrum of the sound pressure level (SPL) for a meanflow velocity of $40\,\mathrm{m/s}$ at $270\,\mathrm{deg}$ in comparison to wind tunnel results the Aeroacoustic Wind tunnel Braunschweig (AWB). The measurement results are corrected by an offset of roughly $+14\,\mathrm{dB}$.

Trailing-Edge Applications," AIAA Paper 2014-3041, 2014.

[7]Slattery, J. C., "Single-phase flow through porous media," *AIChE Journal*, Vol. 15, No. 6, 1969, pp. 866–872.

[8]Whitaker, S., "The transport equations for multi-phase systems," *Chemical Engineering Science*, Vol. 28, No. 1, 1973, pp. 139–147.

[9]Gray, W. G., "A derivation of the equations for multi-phase transport," *Chemical Engineering Science*, Vol. 30, No. 2, 1975, pp. 229–233.

[10]Gray, W. G. and Lee, P. C. Y., "On the theorems for local volume averaging of multiphase systems," *International Journal of Multiphase Flow*, Vol. 3, No. 4, 1977, pp. 333–340.

[11]Hassanizadeh, M. and Gray, W. G., "General conservation equations for multi-phase systems: 1. Averaging procedure," *Advances in Water Resources*, Vol. 2, No. 0, 1979, pp. 131–144.

[12]Hassanizadeh, M. and Gray, W. G., "General conservation equations for multi-phase systems: 2. Mass, momenta, energy, and entropy equations," *Advances in Water Resources*, Vol. 2, No. 0, 1979, pp. 191–203.

[13]Drew, D. A., "Mathematical Modeling of Two-Phase Flow," *Annu. Rev. Fluid Mech.*, Vol. 15, No. 1, 1983, pp. 261–291.

[14]Bear, J. and Corapcioglu, M. Y., editors, *Fundamentals of Transport Phenomena in Porous Media*, NATO ASI Series, Springer Netherlands, 1984.

[15]Ni, J. and Beckermann, C., "A volume-averaged two-phase model for transport phenomena during solidification," *Metallurgical Transactions B*, Vol. 22, No. 3, 1991, pp. 349–361.

[16]Breugem, W. P. and Boersma, B. J., "Direct numerical simulations of turbulent flow over a permeable wall using a direct and a continuum approach," *Physics of Fluids*, Vol. 17, No. 2, 2005, pp. 025103–15.

[17]Liu, Q. and Vasilyev, O. V., "A Brinkman penalization method for compressible flows in complex geometries," *Journal of Computational Physics*, Vol. 227, No. 2, 2007, pp. 946–966.

[18]Ewert, R., Dierke, C. A. J., and Herr, M., "RANS/CAA Based Prediction of NACA0012 Broadband Trailing-Edge Noise and Experimental Validation," AIAA Paper 2009-3269, 2009.

[19]Dierke, J., Appel, C., Siebert, J., and Ewert, R., "A generic computational study of broadband high-lift noise generation for simplified slat and flap problems." AIAA Paper 2012-2102, 2012.

[20]Bauer, M., Dierke, J., and Ewert, R., "Application of a Discontinuous Galerkin Method to Predict Airframe Noise," AIAA Paper 2009-3175, 2009.

[21]Ewert, R., Dierke, J., Appel, C., Pott-Pollenske, M., and Sutcliff, M., "CAA-RPM Prediction and Validation of Slat Setting Influence on Broadband High-Lift Noise Generation," AIAA Paper 2010-3833, 2010.

[22]Ewert, R., Dierke, J., Siebert, J., Neifeld, A., Appel, C., Siefert, M., and Kornow, O., "CAA broadband noise prediction for aeroacoustic design," *Journal of Sound and Vibration*, Vol. 330, No. 17, 2011, pp. 4139–4160.

[23]Ewert, R., Neifeld, A., and Fritzsch, A., "A 3-D modal stochastic jet noise source model," AIAA Paper 2011-2887, 2011.

[24]Neifeld, A. and Ewert, R., "Jet Mixing Noise from Single Stream Jets using Stochastic Source Modeling," AIAA Paper 2011-2700, 2011.

[25]Ewert, R., Neifeld, A., and Wohlbrandt, A., "A three-parameter Langevin model for hot jet mixing noise prediction," AIAA Paper 2012-2238, 2012.

[26]Neifeld, A. and Ewert, R., "On the Contribution of Higher Azimuthal Modes to the Near- and Far-Field of Jet Mixing Noise," AIAA Paper 2012-2114, 2012.

[27]Neifeld, A., Ewert, R., Keller, D., and Steger, M., "Towards Prediction of Jet Noise Installation Effect using Stochastic Source Modeling," AIAA Paper 2014-3059, 2014.

[28]Neifeld, A., Boenke, D., Dierke, J., and Ewert, R., "Jet Noise Prediction with Eddy Relaxation Source Model," AIAA Paper 2014-3059, 2014.

[29]Herr, M., Ewert, R., Rautmann, C., Kamruzzaman, M., Bekiropoulos, D., Iob, A., Arina, R., Batten, P., Chakravarthy, S., and Bertagnolio, F., "Broadband Trailing-Edge Noise Predictions—Overview of BANC-III Results," Aiaa paper, 2015.

[30]Rautmann, C., Dierke, J., Ewert, R., Hu, N., and Delfs, J., "Generic Airfoil Trailing-Edge Noise Prediction using Stochastic Sources from Synthetic Turbulence," AIAA Paper 2014-3298, 2014.

[31]Ewert, R. and Schröder, W., "Acoustic perturbation equations based on flow decomposition via source filtering," *Journal of Computational Physics*, Vol. 188, No. 2, 2003, pp. 365–398.

[32]Crighton, D., Dowling, A. P., Ffowcs Williams, J., Heckl, M., and Leppington, F., *Modern Methods in Analytical Acoustics: Lecture Notes*, Springer Berlin, 1996.

[33]Ascher, U. M., Ruuth, S. J., and Spiteri, R. J., "Implicit-explicit Runge-Kutta methods for time-dependent partial differential equations," *Special Issue on Time Integration*, Vol. 25, No. 2–3, 1997, pp. 151–167.

[34]Boscarino, S. and Russo, S., "On the uniform accuracy of IMEX Runge-Kutta schemes and applications to hyperbolic systems with relaxation," *Communications to SIMAI*, edited by Luigia Puccio, Vol. 2, Società Italiana di Matematica Applicata e Industriale, 2007.

[35]Delfs, J. W., Bauer, M., Ewert, R., Grogger, H. A., Lummer, M., and Lauke, T. G. W., "Numerical Simulation of Aerodynamic Noise with DLR's aeroacoustic code PIANO," 2008.

[36]Ewert, R. and Edmunds, R., "CAA Slat Noise Studies Applying Stochastic Sound Sources Based on Solenoidal Digital Filters," AIAA Paper 2005-2862, 2005.

[37]Ewert, R., "Broadband slat noise prediction based on CAA and stochastic sound sources from a fast random particle-mesh (RPM) method," *Turbulent Flow and Noise Generation*, Vol. 37, No. 4, 2008, pp. 369–387.

[38]Tam, C. K. W. and Webb, J. C., "Dispersion-Relation-Preserving Finite Difference Schemes for Computational Acoustics," *Journal of Computational Physics*, Vol. 107, No. 2, 1993, pp. 262–281.

[39]Lummer, M., Delfs, J. W., and Lauke, T., "Simulation of the influence of trailing edge shape on airfoil sound generation," AIAA Paper 2003-3109, 2003.

[40]Thompson, K. W., "Time dependent boundary conditions for hyperbolic systems," *Journal of Computational Physics*, Vol. 68, No. 1, 1987, pp. 1–24.

[41]Thompson, K. W., "Time-dependent boundary conditions for hyperbolic systems, II," *Journal of Computational Physics*, Vol. 89, No. 2, 1990, pp. 439–461.

[42]Mößner, M. and Radespiel, R., "Numerical Simulations of Turbulent Flow over Porous Media," *21st AIAA Computational Fluid Dynamics Conference*, 2013.

A. PROPERTIES OF VOLUME AVERAGING

One property of volume averaging is that it is interchangeable with summation, i.e.

$$\langle a+b\rangle^{i,s} = \langle a\rangle^{i,s} + \langle b\rangle^{i,s}\,. \tag{43}$$

It follows directly from the definition Eq. (1) (just shown for the superficial component)

$$\langle a+b\rangle^{s} = \frac{\int G\,(a+b)\,d^3x'}{V_\Delta} = \frac{\int G a d^3x'}{V_\Delta} + \frac{\int G b d^3x'}{V_\Delta} = \langle a\rangle^{s} + \langle b\rangle^{s}\,. \tag{44}$$

Commutation of volume averaging and time differentiation follows immediately from the definitions Eqs. (1) and (3), i.e.

$$\left\langle \frac{\partial \rho}{\partial t} \right\rangle^{s} = \frac{1}{V_\Delta}\int \frac{\partial\, G H \rho}{\partial t} d^3x' = \frac{\partial}{\partial t}\frac{1}{V_\Delta}\int G H \rho\, d^3x' = \frac{\partial}{\partial t}\langle\rho\rangle^{s}\,. \tag{45}$$

Commutativity of volume and averaging with respect to spatial differentiation can be also derived from definition Eq. (1),

$$\begin{aligned}\left\langle \frac{\partial \rho v_i}{\partial x_i} \right\rangle^{s} &= \frac{\int G\,(\boldsymbol{x}-\boldsymbol{x}',\Delta)\,\frac{\partial}{\partial x_i'}\left\{\rho v_i(\boldsymbol{x}',t)\right\} H(f(\boldsymbol{x}'))d^3x'}{\int G\,(\boldsymbol{x}-\boldsymbol{x}',\Delta)\,d^3x'} \\ &= \frac{\int G \frac{\partial}{\partial x_i'}\left\{\rho v_i(\boldsymbol{x}',t) H(f(\boldsymbol{x}'))\right\} d^3x'}{\int G d^3x'} - \underbrace{\frac{\int G \rho v_i \frac{\partial f}{\partial x_i'}\delta(f(\boldsymbol{x}'))d^3x'}{\int G d^3x'}}_{(i)}\,.\end{aligned} \tag{46}$$

The Dirac delta function in the second of the finally resulting terms results from the spatial derivation of the Heaviside function, i.e. $\partial/\partial x_i(H(f)) = \delta(f)\partial f/\partial x_i$. The volume integration over the delta function reduces the volume integral to a surface integral over all boundaries between solid and fluid phase, where $f = 0$. Since the gradient of f is normal to the surface, $\partial f/\partial x_i = n_i$—refer to Fig. 1—the wall normal velocity, i.e. the scalar product of velocity with the wall normal, vanishes ($v_n = v_i n_i = 0$) due to the no-slip condition of the velocity and thus the entire second term (i) vanishes.

The remaining terms can be manipulated further, i.e.

$$\begin{aligned}\int G\frac{\partial \rho v_i H(f)}{\partial x_i'}d^3x' &= \underbrace{\int \frac{\partial}{\partial x_i'}\left\{G\rho v_i H(f)\right\}d^3x'}_{Ia} - \underbrace{\int \frac{\partial G}{\partial x_i'}\rho v_i H(f)d^3x'}_{Ib} \\ &= \underbrace{\int \frac{\partial G}{\partial x_i}\rho v_i H(f)d^3x'}_{II} = \underbrace{\frac{\partial}{\partial x_i}\left[\int G\rho v_i H(f)d^3x'\right]}_{III}\end{aligned} \tag{47}$$

In a first step the differentiation has been shifted to the filter kernel. By means of Gauss theorem the first integral (Ia) will vanish, since the filter function decays for large magnitudes of its argument towards zero. Due to the dependence of the filter function on argument $\boldsymbol{x} - \boldsymbol{x}'$, a derivative with respect to x_i' on G can be changed into a derivative with respect to x_i. This has been applied to proceed from Ib to II. In step III, the derivative is shifted out of the integral. Taking into account the last integral, and utilizing that a Gaussian filter function (which is even) satisfies[b]

$$\frac{\partial}{\partial x_i}\int G d^3x' = \int \frac{\partial G}{\partial x_i}d^3x' = -\int \frac{\partial G}{\partial x_i'}d^3x' = 0, \tag{48}$$

it follows

$$\left\langle \frac{\partial \rho v_i}{\partial x_i}\right\rangle^s = \frac{\partial}{\partial x_i}\left\{\langle\rho\rangle^s\left[v_i\right]\right\} = \frac{\partial}{\partial x_i}\langle\rho v_i\rangle^s = \frac{\partial}{\partial x_i}\left\{\frac{\int G\rho v_i H(f)d^3x'}{\int G d^3x'}\right\}. \tag{49}$$

This result proves commutativity of superficial volume averaging and spatial differentiation for the term ρv_i, Eq. (12). Note, strict satisfaction of commutativity is a result of the no-slip condition that causes the vanishing of term (i) in Eq. (46). For other terms this is not in general the case. For example, the previous steps applied to variable pressure p instead of ρv_i yields for this term (i)

$$f_i^p = \frac{\int G\, pn_i\, \delta(f(\boldsymbol{x}'))d^3x'}{V_\Delta} = \frac{1}{V_\Delta}\int\limits_S G\, pn_i\, dS. \tag{50}$$

This represents the pressure force from the solid onto the fluid. Consequent application of the volume averaging procedure to the continuity and momentum equation yields

$$\left\langle \frac{\partial \rho}{\partial t} + \frac{\partial \rho v_i}{\partial x_i}\right\rangle^s = \frac{\partial\langle\rho\rangle^s}{\partial t} + \frac{\partial}{\partial x_i}\left\{\langle\rho\rangle^s\left[v_i\right]\right\} = 0 \tag{51}$$

and

$$\begin{aligned}&\left\langle \frac{\partial \rho v_i}{\partial t} + \frac{\partial \rho v_i v_j}{\partial x_j} + \frac{\partial p}{\partial x_i} - \frac{\partial \tau_{ij}}{\partial x_j}\right\rangle^s = \\ &\frac{\partial\langle\rho\rangle^s\left[v_i\right]}{\partial t} + \frac{\partial\langle\rho\rangle^s\left[v_i\right]\left[v_j\right]}{\partial x_j} + \frac{\partial\langle p\rangle^s}{\partial x_i} - \frac{\partial\langle\tau_{ij}\rangle^s}{\partial x_j} - \mathcal{F}_i = 0\end{aligned} \tag{52}$$

with

$$\mathcal{F}_i = f_i - \underbrace{\frac{\partial(\rho v_i v_j - \langle\rho\rangle^s\left[v_i\right]\left[v_j\right])}{\partial x_j}}_{SFS}. \tag{53}$$

[b]The property Eq. (48) would not hold in general for intrinsic volume averaged quantities, since for the denominator $\partial/\partial x_i \int GH(f)\mathrm{d}^3x'$ it cannot be guaranteed that it is always identical zero.

Here the interchangeability of volume averaging and summation has been applied. Furthermore, for all gradient terms commutativity of volume averaging and differentiation has been used.

The volume force f_i represents the effect of term (i) from pressure p as shown by Eq. (50) and a similar shear stress contribution from τ_{ij}. Due to the no-slip condition satisfied by velocity, the term $\rho v_i v_j$ will provide no contribution to f_i. Note, volume averaging in general creates the sub-filter stress (SFS) indicated above from the sub-filter velocity fluctuations $v_i'' = v_i - [v_i]$. The sub-filter velocity component must be distinguished from the Favre fluctuations of the volume averaged velocity defined in Eq. (18). To be precise, the complete velocity is given by

$$v_i = \widetilde{[v_i]} + [v_i]'' + v_i''. \tag{54}$$

The volume force term and sub-filter contributions inside the porous medium are modeled by the ansatz proposed by Darcy and Forchheimer. The Darcy terms describes a velocity proportional volume force, whereas the Forchheimer term explicitly addresses a quadratic contribution to the force,

$$-\mathcal{F}_i = \underbrace{\phi \frac{\langle \mu \rangle^s}{\kappa} [v_i]}_{\text{Darcy terms}} + \underbrace{\langle \rho \rangle^s \, \phi^2 \frac{c_\mathrm{F}}{\sqrt{\kappa}} \sqrt{[v_k][v_k]} [v_i]}_{\text{Forchheimer terms}} \quad , \tag{55}$$

where ϕ denotes the porosity, μ is the dynamic viscosity, κ identifies the permeability and the Forchheimer coefficient is indicated by c_F.

Despite the additional terms, the resulting momentum equation corresponds formally with the Navier-Stokes equations in conservative form. They can be reformulated in primitive form. For example, the momentum equation is rewritten into an equation for the time derivative of velocity by removing with the help of the continuity equation the time derivative of density. The independent variables can be split further into resolved Favre averaged and fluctuating components for the velocity, i.e. Eq. (18), and mean and fluctuating components for pressure and density as defined by Eq. (16). Introducing the decomposition into the equations in primitive notation yields non-linear equations in disturbance form. Next, mean flow terms can be neglected by subtracting the mean of a disturbance equation from itself. Finally, non-linear terms might be neglected. This way, the governing equations can be reformulated into perturbation form as shown in Section II.B. For example, the volume averaged continuity equations is rewritten as

$$\frac{\partial \langle \rho' \rangle^{s'}}{\partial t} + \frac{\partial}{\partial x_i} \left\{ \langle \rho \rangle^{s'} \widetilde{[v_i]} + \overline{\langle \rho \rangle^s} \, [v_i]'' \right\} = 0 \tag{56}$$

Utilizing the notation as introduced by Eqs. (22) and (23), the previous equation agrees with Eq. (24). For the derivation of the momentum equation in the form used in the LPE (with some left-hand side terms shifted to the right-hand side to define appropriate vortex sound sources), the Darcy and Forchheimer terms have to be linearized as well, finally yielding the equation as outlined in Eq. (25). The LPE pressure equation is obtained in the same spirit.

It may be emphasized (without explicit proof) that for a Gaussian filter function

$$G_\Delta \left(\boldsymbol{x} - \boldsymbol{x}', \Delta \right) = \frac{1}{(2\pi)^{3/2} \, \Delta^3} \exp \left[- \frac{|\boldsymbol{x} - \boldsymbol{x}'|^2}{2\Delta^2} \right], \tag{57}$$

the consecutive application of volume averaging to variable a with different length scales for each filter step, i.e.

$$\left\langle \langle a \rangle^s_{\Delta_1} \right\rangle^s_{\Delta_2} = \frac{1}{V_{\Delta_2}} \int G_{\Delta_2} \left\{ \frac{1}{V_{\Delta_1}} \int G_{\Delta_1} a d^3x'' \right\}, d^3x' \tag{58}$$

is equal to one filter step with length scale $\Delta_1 + \Delta_2$, i.e.

$$\left\langle \langle a \rangle^s_{\Delta_1} \right\rangle^s_{\Delta_2} = \langle a \rangle^s_{\Delta_1 + \Delta_2} \, . \tag{59}$$

For $\Delta_1 \to 0$ the first filter would represent a Dirac delta function, that is applicable for a pore size tending to zero, i.e. $D_p \to 0$. Consequently, volume averaged (mean and fluctuating) quantities based on length scale Δ_2 can be obtained by consecutively volume average quantities initially obtained from volume averaging with $\Delta_1 \to 0$ with a filter of length scale Δ_2.